Minimal East Antarctic Ice Sheet retreat onto land during the past 8 million years

Jeremy D. Shakun¹, Lee B. Corbett², Paul R. Bierman², Kristen Underwood³, Donna M. Rizzo³, Susan R. Zimmerman⁴, Marc W. Caffee^{5,6}, Tim Naish⁷, Nicholas R. Golledge⁷, Carling C. Hay¹

¹Department of Earth and Environmental Sciences, Boston College, Chestnut Hill, MA 02467, USA

²Department of Geology and Rubenstein School of the Environment and Natural Resources, University of Vermont, Burlington, VT 05405, USA

³Civil and Environmental Engineering, University of Vermont, Burlington, VT 05405, USA
 ⁴Center for Accelerator Mass Spectrometry, Lawrence Livermore National Laboratory,
 Livermore, CA 94550, USA

⁵Department of Earth, Atmospheric, and Planetary Sciences, Purdue University, West Lafayette, IN 47907, USA

⁶Department of Physics and Astronomy, Purdue University, West Lafayette, IN 47907, USA ⁷Antarctic Research Centre, Victoria University of Wellington, Wellington, New Zealand.

The East Antarctic Ice Sheet (EAIS) is the largest potential contributor to future sea level rise, but projections are hindered by uncertainty in how the EAIS responded to past warm periods, for example during the Pliocene (5.3-2.6 Myr ago) when atmospheric CO₂ concentrations were last \geq 400 ppm. Geological evidence indicates that some marine-based portions of the EAIS and West Antarctic Ice Sheet (WAIS) retreated during parts of the Pliocene^{1,2}, but it remains uncertain whether ice grounded above sea level also experienced retreat. This uncertainty persists because global sea level estimates for the Pliocene have large uncertainties and cannot be used to rule out substantial terrestrial ice loss³, and also because direct geological evidence bearing on past ice retreat on land is lacking. Here, we show that land-based sectors of the EAIS draining into the Ross Sea were ice covered throughout the past 8 Myr based on extremely low concentrations of cosmogenic ¹⁰Be and ²⁶Al in quartz sand extracted from a land-proximal marine sediment core. The sediment we analyzed was eroded from the continent where it experienced only minimal exposure to cosmic radiation, indicating that atmospheric warming during the past 8 Myr was insufficient to cause widespread and/or long-lasting meltback of the EAIS margin onto land. We suggest that Antarctic ice volume variations in response to the range of global temperature experienced over this period – up to 2-3°C above preindustrial⁴, which correspond to future scenarios with CO₂ concentrations between 400 and 500 ppm – are instead driven mostly by retreat of marine ice margins, in agreement with the latest models^{5,6}.

The configuration of the EAIS during the Pliocene is a longstanding topic of debate (ref. 7 and references therein). Although the marine δ^{18} O record is consistent with permanent EAIS establishment after 14 Ma, Pliocene marine diatoms from glacial sediments high in the

Transantarctic Mountains (TAM) first raised the possibility that the ice sheet significantly retreated, resulting in an interior seaway, and subsequently regrew as recently as 3 Ma. In apparent contradiction, geomorphic investigations identified ancient land surfaces in the TAM, implying persistent polar desert conditions for the past several million years, and, together with evidence that the diatoms were not in situ but rather wind transported, doubts developed around the scale of a late Neogene deglaciation. More recently, land-proximal marine sediment records revealed significantly warmer than present sea surface temperatures, a lack of summer sea ice, and retreat of marine-based parts of the EAIS and WAIS numerous times during the Pliocene^{1,2,8}.

Recent modeling may reconcile these seemingly disparate observations, suggesting that marine-based ice sheet retreat during the Pliocene allowed winds to loft diatoms from isostatically-uplifted marine sediments onto TAM tills that may in fact be much older^{8,9}. Atmospheric warming in these Pliocene simulations is insufficient to drive widespread surface melting and retreat of land-terminating ice margins. Nonetheless, the resolution of the models is coarse relative to the width of potential ablation zones on the steep flanks of the ice sheet, and observations show widespread surface melt around Antarctica as high as 1300 m asl even in the current climate¹⁰. Moreover, Pliocene sea-level reconstructions cannot exclude the possibility of EAIS margin retreat onto land. Global sea-level estimates for Pliocene interglacials range from 5 to >40 m higher than today^{3,11}, owing to persistent uncertainties associated with extracting the sea-level signal from the marine δ^{18} O record and paleo-shorelines, in part due to dynamic topographic changes and isostatic adjustment over time³. While most of this sea-level rise could be accounted for by loss of the current Greenland Ice Sheet (7 m) and/or marine-based portions of the WAIS (3 m) and EAIS (19 m), the highest estimates would also require input from EAIS

land-based sectors (34 m)¹². To date, there has been no direct evidence confirming whether the EAIS margin retreated onto land during the past several million years.

Here, we directly test for retreat onto land of the EAIS margin and consequent exposure of the land surface to cosmic rays over the past 8 Myr by measuring concentrations of the cosmogenic nuclides ¹⁰Be and ²⁶Al in quartz sands from the AND-1B sediment core retrieved from beneath the Ross Ice Shelf (Fig. 1a, 2c). While diatom-rich units in AND-1B were previously used to identify numerous open-water intervals¹, likely associated with collapse of the WAIS⁸, we focused on terrigenous sediments from the intervening glacial units (Fig. 2) sourced from the EAIS. Cosmogenic nuclides are well suited to evaluating past terrestrial retreat of the EAIS because they are diagnostic of subaerial land exposure; these nuclides do not form in measurable concentrations under ice sheets, which shield rock surfaces from cosmic radiation. Cosmogenic nuclide concentrations in terrestrial materials from glaciated regions are controlled by a combination of ice sheet extent and erosional processes¹³. Nuclide production is highest at the ground surface, decreases exponentially in the top few meters, and then extends tens of meters further at much lower rates¹⁴. Exposure drives nuclide concentrations higher with time, while nuclides are lost due to decay (10 Be $t_{1/2} = 1.39$ Myr; 26 Al $t_{1/2} = 0.71$ Myr) and erosion that strips nuclide-rich surface material. Glaciation tends to favor both of these concentrationlowering processes because it halts production and, under areas of erosive ice, removes previously exposed material from the bed. The nuclide concentration preserved in sediments carried from land to an adjacent ocean reflects a convolution of exposure and burial history along with erosion depth, integrated along ice flow lines and weighted by erosion rate¹³.

The AND-1B sediments we measured likely represent a relatively large area well upstream of the core site. Sand provenance indicators suggest that AND-1B glaciogenic

sediments were probably sourced from the Skelton and Mulock Glacier region of the TAM throughout the Plio-Pleistocene¹⁵, and perhaps also the Wilkes Basin further inboard beneath the EAIS (Fig. 1). Indeed, Last Glacial Maximum tills further outboard in the Ross Sea appear to have derived from the ice sheet interior as well as along the entire width of the TAM traversed by outlet glaciers¹⁶. Modeling suggests that outlet glaciers may have been more active during past warm periods, sliding and eroding along much of their lengths¹⁷, and erosive zones would have migrated inward as the ice sheet margin retreated (Extended Data Fig. 1). The volcanic rocks in McMurdo Sound surrounding the core site do not contain quartz¹⁵, precluding a local contribution. These source areas would have likely accumulated cosmogenic nuclides if substantial ice loss occurred in the past. The TAM are above sea level and would experience cosmic ray exposure during ice-free periods. The Wilkes Basin lies below sea level today¹², but much of it would have rebounded above sea level had the ice sheet experienced major retreat (Fig. 1a; Extended Data Fig. 2).

We evaluated whether AND-1B sediments have high cosmogenic nuclide concentrations indicative of past ice retreat using 62 diamictite samples from the top 786 m of the core; these were amalgamated and purified to obtain sufficient quartz sand for measurement, yielding eight samples (designated A-H, from top to bottom), which span core intervals of 0.2-260.7 m in thickness or 0.002-2.166 Myr in duration (Fig. 2) (Methods; Supplementary Data). Procedural blanks extracted along with samples quantify background nuclide abundances characteristic of sample processing and AMS analysis (Methods; Supplementary Data).

In general, AND-1B nuclide concentrations are only marginally higher than procedural blanks, particularly for ²⁶Al (Fig. 3); thus, they are indicative of little if any near-surface exposure. We used several statistical techniques to evaluate the certainty with which sample

measurements exceeded analytical backgrounds. First, cumulative frequency distributions suggest that the sample population as a whole contains low but measurable concentrations of both 10 Be and 26 Al (Extended Data Fig. 3). Then, we used both Frequentist and Bayesian statistical approaches to consider whether individual samples contain cosmogenic nuclides at concentrations above background (Methods; Extended Data Table 2). We find that all but the oldest sample contain more 10 Be than process blanks. Six of eight samples (B, C, E, F, G, H) contain 26 Al above blank level. We corrected sample nuclide concentrations for background using blank values and for decay on the seafloor using the core age model (Methods). Although the 26 Al 10 Be ratio can be used to monitor burial duration after exposure because the faster decay of 26 Al relative to 10 Be causes the ratio to decrease from its production value 14 , the relatively large uncertainties of the low-concentration AND-1B data preclude resolution of meaningful decay-corrected 26 Al 10 Be ratios.

The presence of ¹⁰Be and ²⁶Al in AND-1B sediments provides unequivocal evidence for past landscape exposure in source regions. The relatively short half-life of ²⁶Al requires that this exposure occurred after EAIS expansion at 14 Ma, otherwise none would remain today (Extended Data Fig. 4). However, decay-corrected nuclide concentrations are extremely low, declining from only ~12,000 to 600 ¹⁰Be atoms g⁻¹ and 120,000 to 6,000 ²⁶Al atoms g⁻¹ over the Plio-Pleistocene (Fig. 4a; Extended Data Fig. 4) – the equivalent of only 150-3,000 years of surface exposure at sea level (where the ¹⁰Be production rate is 4 atoms g⁻¹ yr⁻¹) and even less at higher elevations. It is possible that these small concentrations of nuclides result from incorporation of minor amounts of material derived from nunataks in the TAM¹⁸. In any case, these low concentrations are evidence that any Pliocene land-based ice sheet retreat upstream

from AND-1B was at most very limited in duration and/or extent. Several arguments support this interpretation.

First, modeling suggests that, in most plausible scenarios, AND-1B nuclide concentrations are consistent with spatially and/or temporally limited ice retreat during glacial cycles of the Pliocene and especially the Pleistocene (Methods); repeated exposures, even if relatively brief, would have led to higher concentrations than we measured (Extended Data Fig. 5). A single, long-lasting Pliocene exposure event on the other hand, such as during the warm ~3.6-3.4 Ma interval implied by a 60-m thick diatomite in the AND-1B core¹, could yield ¹⁰Be concentrations consistent with our Pliocene data if erosion rates were at least tens of meters per million years once the ice cover returned. However, such high erosion rates cause ¹⁰Be concentrations to decline more steeply over time than observed in our record without continued exposures (Extended Data Fig. 6 and 7), and frequent exposure seems unlikely given that temperatures and sea level were rarely higher than today during the Pleistocene^{19,20}. The decreasing trend in AND-1B nuclide concentrations instead nearly follows a decay curve (Fig. 4a), a trend most consistent with low rates of bedrock erosion under continuous ice cover since the last episodes of exposure.

The persistent ice cover suggested by our record is also consistent with the perennially frozen conditions that some have argued are needed to explain extreme landscape stability in the TAM over the past several Myr reflected by high cosmogenic nuclide concentrations in exposed surfaces and intact surficial ash deposits⁷.

Lastly, relative stability of the EAIS is evident when the AND-1B cosmogenic marine sediment record is compared to similar records from other ice sheets. Decay-corrected AND-1B ¹⁰Be concentrations are several times lower than values for Greenlandic sediment over the same

time period¹³ (Plio-Pleistocene averages of 7,000 and 25,000 atoms g⁻¹, respectively), which are in turn several times lower than tills from the Laurentide Ice Sheet^{21,22} (Pleistocene average of 70,000 atoms g⁻¹). These patterns are consistent with repeated North American interglacial exposure sustaining higher nuclide concentrations, a generally present but dynamic Greenland Ice Sheet, and persistent Antarctic ice cover maintaining low ¹⁰Be concentrations.

How well does AND-1B represent the broader EAIS? Models simulating EAIS deglaciation suggest that ice may linger in the higher elevations of the TAM, but all show the ice sheet generally contracting inward, with considerable land area currently upstream of the core site exposed relatively early during retreat^{23,24}. Furthermore, these models suggest that warming consistent with even the strongest interglacials of the past 8 Myr would have produced minimal land exposure around the entire EAIS margin^{6,8}. The near absence of cosmogenic nuclides in our record therefore rules out substantial and long-lasting EAIS retreat onto land over the past 8 Myr; a finding consistent with recent seismic imaging off the Aurora Basin²⁵ and that could be confirmed by similar cosmogenic nuclide measurements in cores elsewhere around Antarctica. Our results put an upper limit on estimates of Pliocene sea level, since melting of all marinebased ice in Antarctica¹² and the Greenland Ice Sheet could contribute at most 30 m of sea level rise. Together with prior evidence for open waters at the AND-1B site during the Pliocene¹, our findings agree with model simulations that the terrestrial EAIS experiences minimal melt when CO₂ is near its present value of ~400 ppm for extended periods of time, whereas some marinebased ice sheet sectors largely disappear^{5,23} (Fig. 1c and 4c).

Naish, T. *et al.* Obliquity-paced Pliocene West Antarctic ice sheet oscillations. *Nature* **458**, 322-328, doi:10.1038/nature07867 (2009).

- Cook, C. P. *et al.* Dynamic behaviour of the East Antarctic ice sheet during Pliocene warmth. *Nature Geosci* **6**, 765-769, doi:10.1038/ngeo1889 (2013).
- Dutton, A. *et al.* Sea-level rise due to polar ice-sheet mass loss during past warm periods. *Science* **349**, doi:10.1126/science.aaa4019 (2015).
- Haywood, A. M., Dowsett, H. J. & Dolan, A. M. Integrating geological archives and climate models for the mid-Pliocene warm period. *Nature Communications*, doi:10.1038/ncomms10646 (2016).
- DeConto, R. M. & Pollard, D. Contribution of Antarctica to past and future sea-level rise.

 Nature **531**, 591-597, doi:10.1038/nature17145 (2016).
- Golledge, N. R. *et al.* Antarctic climate and ice-sheet configuration during the early Pliocene interglacial at 4.23 Ma. *Clim. Past* **13**, 959-975, doi:10.5194/cp-13-959-2017 (2017).
- Barrett, P. J. Resolving views on Antarctic Neogene glacial history the Sirius debate.

 Earth and Environmental Science Transactions of the Royal Society of Edinburgh 104,

 31-53, doi:10.1017/S175569101300008X (2013).
- 8 Pollard, D. & DeConto, R. M. Modelling West Antarctic ice sheet growth and collapse through the past five million years. *Nature* **458**, 329-332 (2009).
- 9 Scherer, R. P., DeConto, R. M., Pollard, D. & Alley, R. B. Windblown Pliocene diatoms and East Antarctic Ice Sheet retreat. 7, 12957, doi:10.1038/ncomms12957 (2016).
- Kingslake, J., Ely, J. C., Das, I. & Bell, R. E. Widespread movement of meltwater onto and across Antarctic ice shelves. *Nature* **544**, 349-352, doi:10.1038/nature22049 (2017).
- Raymo, M., Mitrovica, J. X., O'Leary, M. J., DeConto, R. & Hearty, P. Departures from eustasy in Pliocene sea-level records. *Nature Geoscience* **4**, 328-332 (2011).

- Fretwell, P. *et al.* Bedmap2: improved ice bed, surface and thickness datasets for Antarctica. *The Cryosphere* **7**, 375-393, doi:10.5194/tc-7-375-2013 (2013).
- Bierman, P. R., Shakun, J. D., Corbett, L. B., Zimmerman, S. R. & Rood, D. H. A persistent and dynamic East Greenland Ice Sheet over the past 7.5 million years. *Nature* **540**, 256-260, doi:10.1038/nature20147 (2016).
- Gosse, J. C. & Phillips, F. M. Terrestrial in situ cosmogenic nuclides: theory and application. *Quaternary Science Reviews* **20**, 1475-1560 (2001).
- Talarico, F. M., McKay, R. M., Powell, R. D., Sandroni, S. & Naish, T. Late Cenozoic oscillations of Antarctic ice sheets revealed by provenance of basement clasts and grain detrital modes in ANDRILL core AND-1B. *Global and Planetary Change* **96**, 23-40 (2012).
- Farmer, G. L. & Licht, K. J. Generation and fate of glacial sediments in the central Transantarctic Mountains based on radiogenic isotopes and implications for reconstructing past ice dynamics. *Quaternary Science Reviews* **150**, 98-109 (2016).
- Golledge, N. R. & Levy, R. H. Geometry and dynamics of an East Antarctic Ice Sheet outlet glacier, under past and present climates. *Journal of Geophysical Research: Earth Surface* **116**, doi:10.1029/2011JF002028 (2011).
- Jones, R. S. *et al.* Cosmogenic nuclides constrain surface fluctuations of an East

 Antarctic outlet glacier since the Pliocene. *Earth and Planetary Science Letters* **480**, 7586, doi:doi.org/10.1016/j.epsl.2017.09.014 (2017).
- Rohling, E. J. *et al.* Sea-level and deep-sea-temperature variability over the past 5.3 million years. *Nature* **508**, 477-482, doi:10.1038/nature13230 (2014).

- 20 Snyder, C. W. Evolution of global temperature over the past two million years. *Nature* **538**, 226-228, doi:10.1038/nature19798 (2016).
- Balco, G., Stone, J. O. & Jennings, C. Dating Plio-Pleistocene glacial sediments using the cosmic-ray-produced radionuclides Be-10 and Al-26. *American Journal of Science* **305**, 1-41 (2005).
- Rovey, C. W. & Balco, G. Paleoclimatic interpretations of buried paleosols within the pre-Illinoian till sequence in northern Missouri, USA. *ppp* **417**, 44-56 (2015).
- Gasson, E., DeConto, R. M., Pollard, D. & Levy, R. H. Dynamic Antarctic ice sheet during the early to mid-Miocene. *Proceedings of the National Academy of Sciences* **113**, 3459-3464, doi:10.1073/pnas.1516130113 (2016).
- Winkelmann, R., Levermann, A., Ridgwell, A. & Caldeira, K. Combustion of available fossil fuel resources sufficient to eliminate the Antarctic Ice Sheet. *Science Advances* 1, doi:10.1126/sciadv.1500589 (2015).
- Gulick, S. P. S. *et al.* Initiation and long-term instability of the East Antarctic Ice Sheet. *Nature* **552**, 225, doi:10.1038/nature25026 (2017).
- 26 Hay, C. *et al.* The sea-level fingerprints of ice-sheet collapse during interglacial periods. *Quaternary Science Reviews* **87**, 60-69, doi:doi.org/10.1016/j.quascirev.2013.12.022

 (2014).
- Wilson, G. S. *et al.* Neogene tectonic and climatic evolution of the Western Ross Sea,

 Antarctica Chronology of events from the AND-1B drill hole. *Global and Planetary Change* **96**, 189-203 (2012).

- Zachos, J., Pagani, M., Sloan, L., Thomas, E. & Billups, K. Trends, Rhythms, and Aberrations in Global Climate 65 Ma to Present. *Science* **292**, 686-693, doi:10.1126/science.1059412 (2001).
- 29 Luthi, D. *et al.* High-resolution carbon dioxide concentration record 650,000-800,000 years before present. *Nature* **453**, 379-382 (2008).
- Foster, G. L., Royer, D. L. & Lunt, D. J. Future climate forcing potentially without precedent in the last 420 million years. **8**, 14845, doi:10.1038/ncomms14845 (2017).

Supplementary Information is available in the online version of the paper.

Acknowledgments We thank the Antarctic Research Facility for AND-1B samples, and Jerry X. Mitrovica for his help performing the glacial isostatic adjustment modeling. Research supported by NSF ARC-1023191 (PB, LC), Boston College start-up funds (JS), Vermont EPSCoR Grant Nos. EPS-1101317 and NSF OIA 1556770 (KU, DR), NSF EAR-1153689 (MC), and the New Zealand Ministry of Business Innovation and Employment Contract C05X1001 (TN, NG). This is LLNL-JRNL-735619.

Author Contributions J.D.S. and P.R.B. conceived the study. L.B.C. performed laboratory work. K.U. and D.M.R. conducted statistical analyses. S.R.Z. and M.W.C. made isotopic measurements. T.R.N. and N.R.G. contributed to data interpretation. C.C.H. performed glacial isostatic adjustment simulations. All authors contributed to the preparation of the manuscript.

Author Information Reprints and permissions information is available at www.nature.com/reprints. The authors declare no competing financial interests. Readers are welcome to comment on the online version of the paper. Publisher's note: Spring Nature remains neutral with regard to jurisdictional claims in published maps and institutional affiliations.

Correspondence and requests for material should be addressed to J.D.S.

(jeremy.shakun@bc.edu).

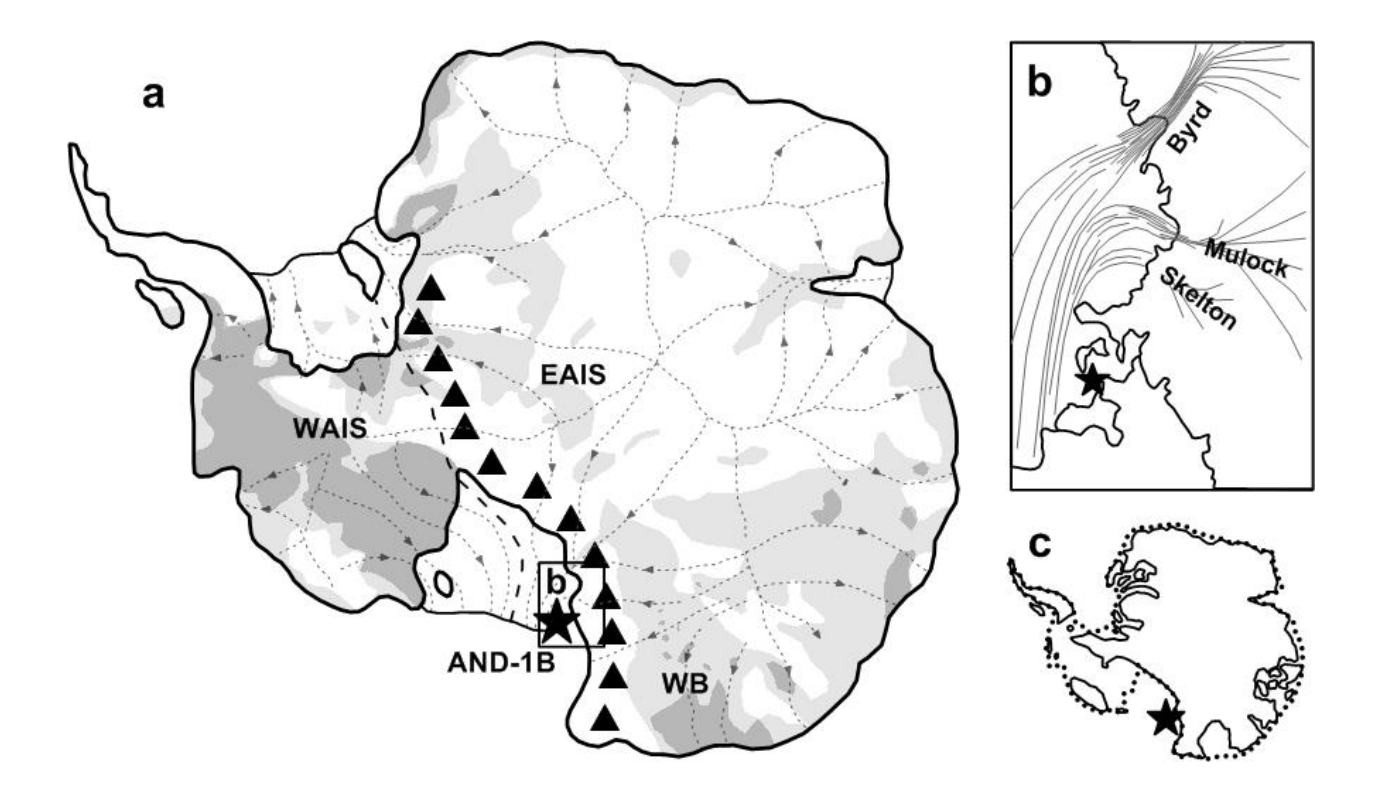


Figure 1. Location of the AND-1B core in the Ross Sea, ice flow lines to the core site, and simulated ice sheet retreat during the Pliocene. (a) Some areas upstream of the core site are currently below sea level 12 (light gray), but would mostly rise above sea level 10 kyr after deglaciation of marine-based ice sheet sectors²⁶ (dark gray) and be exposed to cosmic radiation.

WB = Wilkes Basin, and triangles represent the Transantarctic Mountains. Figure modified from ref. 1. (b) Ice currently flows to the core site from the Skelton and Mulock outlet glaciers of the EAIS, and likely did throughout the Plio-Pleistocene¹⁵. Figure modified from ref. 15. (c)

Simulated Pliocene ice sheet configuration from ref. 5 (solid line), with retreat restricted almost entirely to marine-based sectors of the ice sheet. Dashed line shows current ice extent. Star shows location of the AND-1B site in all panels.

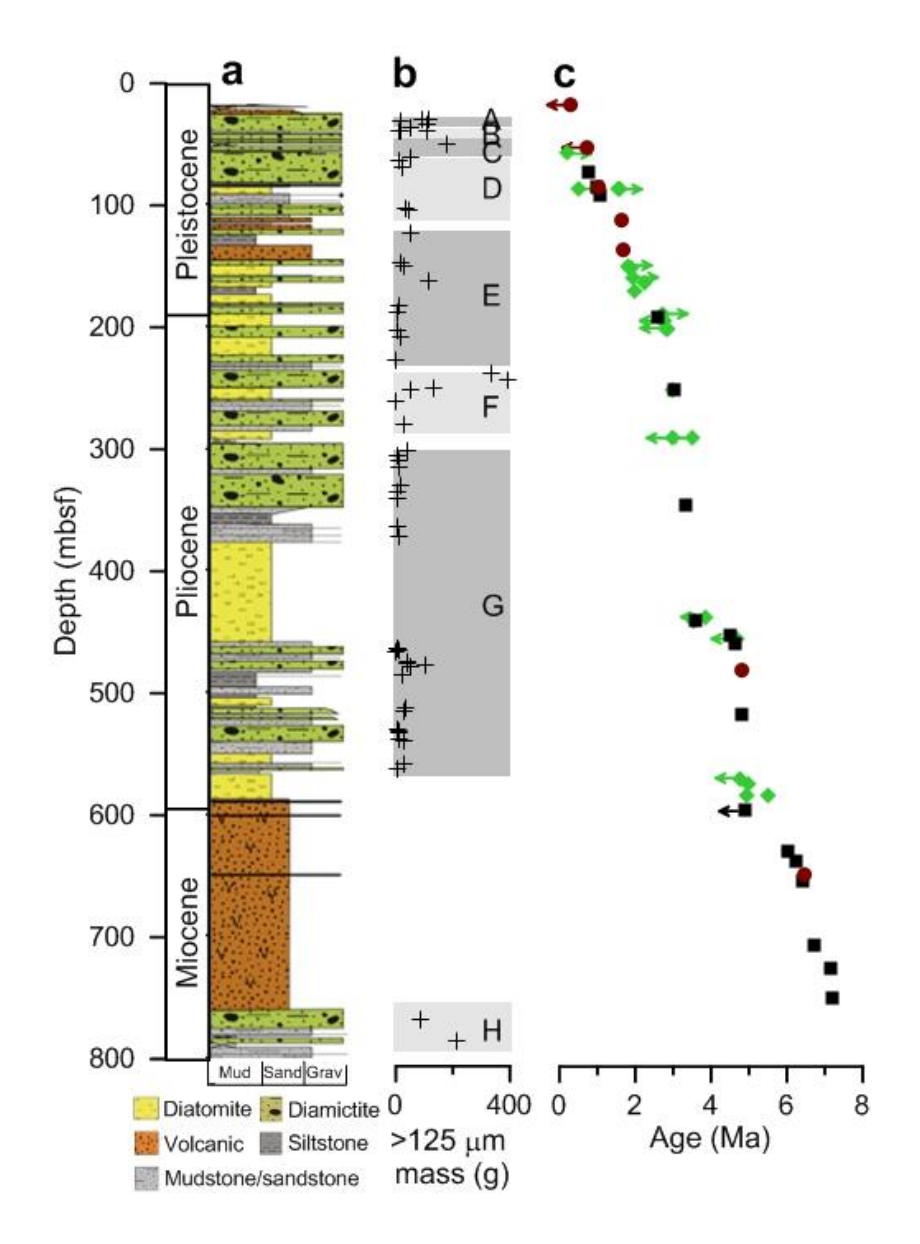


Figure 2. AND-1B stratigraphy and cosmogenic nuclide samples. (a) Core lithostratigraphy²⁷. (b) Sand masses of 62 samples used in this study (crosses) (Supplementary Data). Quartz was extracted from these samples and amalgamated, yielding eight final samples used for cosmogenic nuclide measurement labeled A-H (gray shaded intervals). Note that there is a ~200 m gap between samples G and H. (c) Age control points from paleomagnetic events (black squares), ⁴⁰Ar/³⁹Ar ages (maroon circles), and diatom datums (green diamonds)²⁷. Arrows designate maximum or minimum limiting ages.

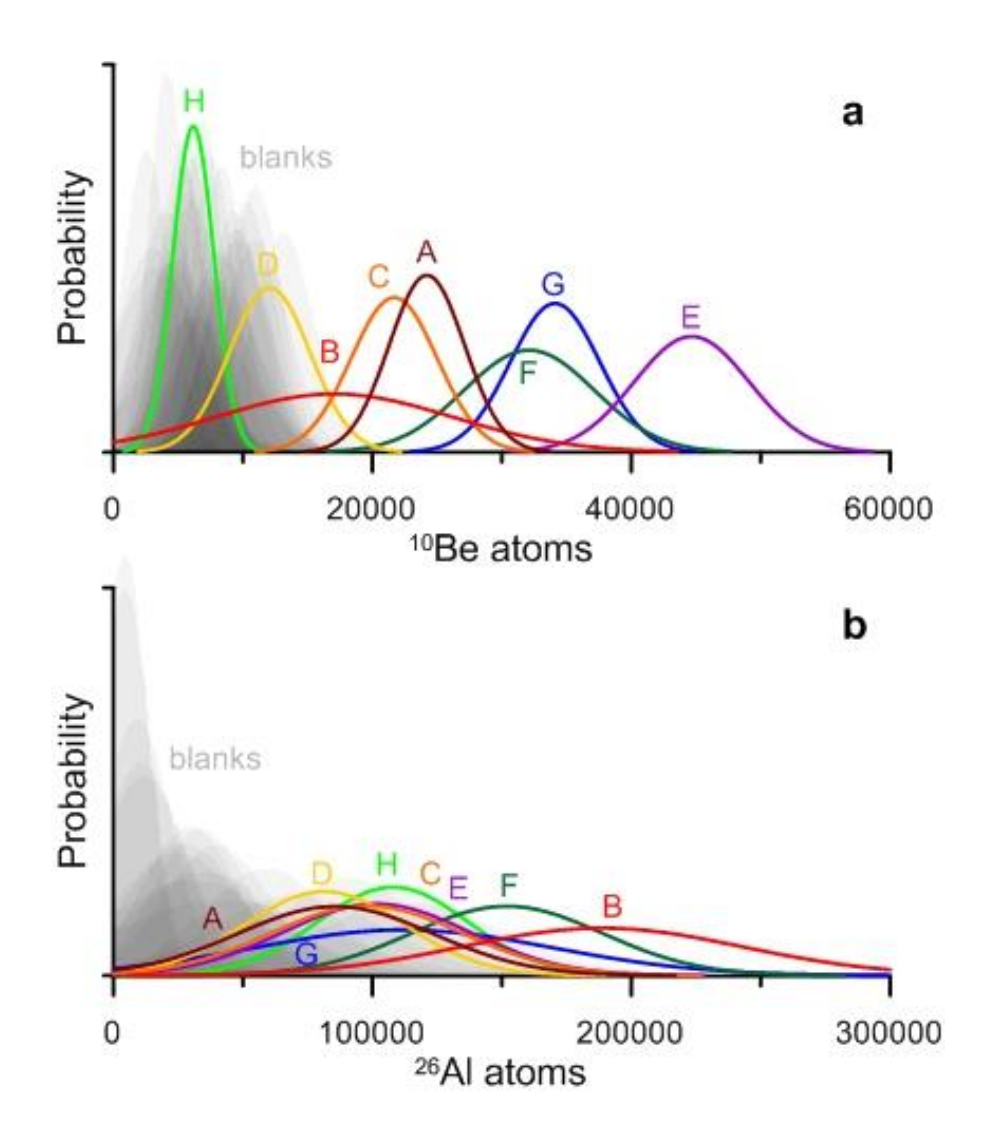


Figure 3. Cosmogenic nuclide abundances. Probability distribution functions of (a) ¹⁰Be and (b) ²⁶Al abundances (total number of atoms) measured in AND-1B samples (colored lines) as well as all laboratory process blanks run alongside low-level samples in the same hood by the same operator (shown as translucent gray rather than lines for visual clarity). Labels A-H give sample names from top to bottom in the core, and asterisks denote samples that have nuclide abundances above blank level at 90% confidence according to Bayesian analysis (Methods). Note that the x-axes in the two panels have different scales.

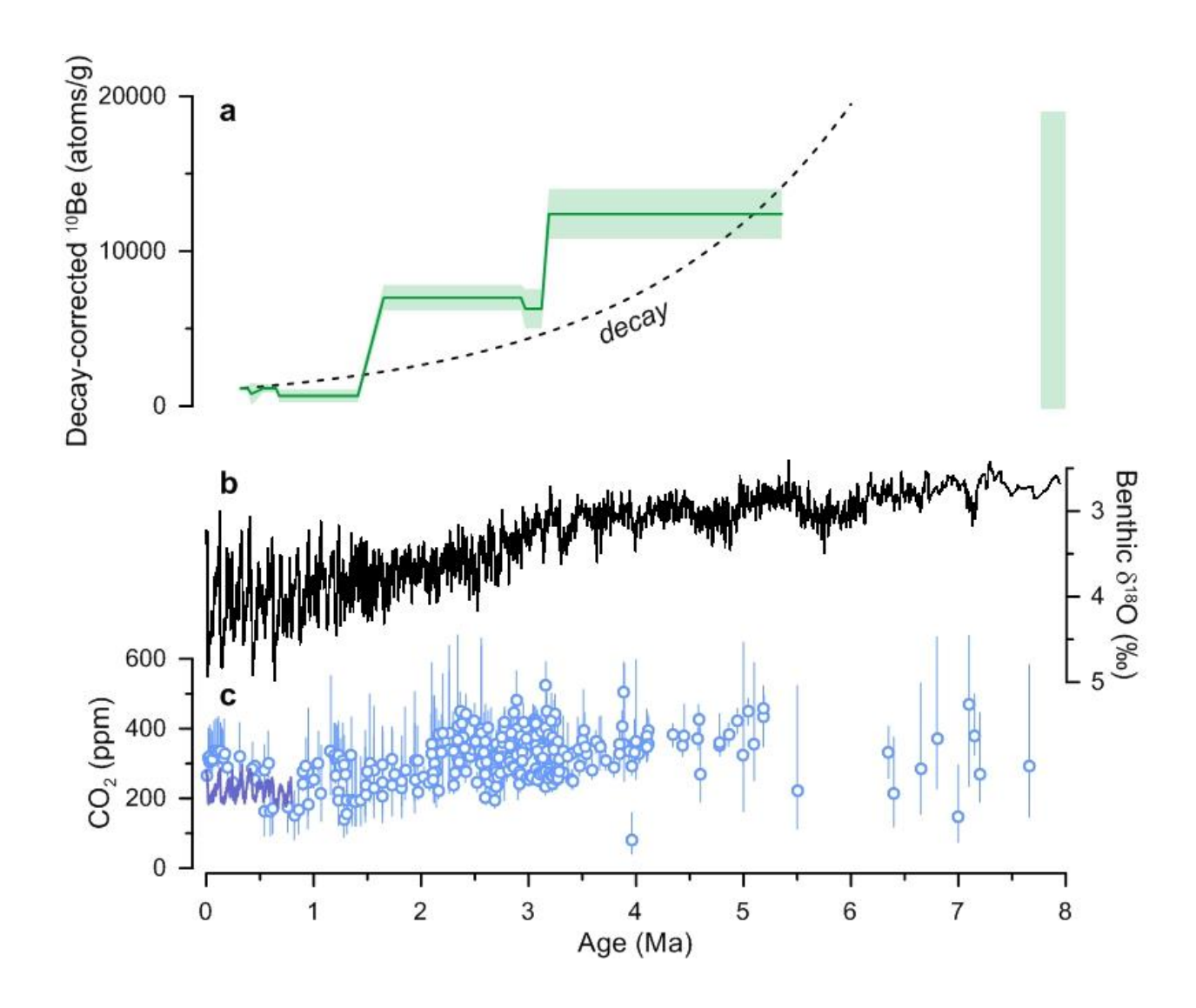


Figure 4. AND-1B ¹⁰Be record. (a) Decay-corrected ¹⁰Be concentrations from AND-1B. Shading shows 1σ uncertainty, and the green bar near 8 Ma represents the possible range of decay-corrected concentrations in the oldest AND-1B sample that is now below detection limit. The dashed black line shows the decay curve that would end at the youngest AND-1B sample.

(b) Benthic δ¹⁸O record, a proxy for global ice volume and deep ocean temperature²⁸. (c) Atmospheric CO₂ concentrations from ice cores²⁹ (purple line), and paleosol δ¹³C (red), alkenone δ¹³C (yellow), stomata (green), and marine δ¹¹B (blue) with 1σ uncertainties³⁰.

Methods

Sediment samples. We prepared a total of 62 samples ranging in thickness from 2 to 70 cm from the top 786 m of the AND-1B core. The top 61 samples are from Facies 10, diamicton interpreted as subglacial sediments, though possibly also associated with rainout from floating ice and mass flows³¹. The lowest sample is from Facies 4, interpreted as hemipelagic muds and clasts rained out from icebergs and/or an ice shelf³¹. The samples were disaggregated by soaking in weak acid, wet sieved, and then due to their small masses, the >125 μm fractions from adjacent samples were amalgamated until they totaled ~200 g, yielding 14 samples. Quartz was isolated through an initial heated HCl ultrasonic etching followed by repeated weak (0.25%) HF/HNO₃ etching, and the >1000 μm fraction was sieved to remove larger grains feed up during acid disaggregation. Because some of the resulting quartz separates were too small for ¹⁰Be measurement, we amalgamated adjacent samples once again, producing eight final samples with quartz masses of 14-20 g spanning core intervals of 0.2-260.7 m in thickness, or 0.002-1.763 Myr in duration. Sample processing details are given in Supplementary Data.

Cosmogenic nuclide extraction. ¹⁰Be and ²⁶Al were extracted from quartz at the University of Vermont following the methods of Corbett et al.³². We added ~250 μg of ⁹Be to each sample using a beryl carrier made at University of Vermont. Total ²⁷Al was quantified using inductively coupled plasma optical emission spectrometry analysis of replicate aliquots removed from samples directly following digestion; measurements were made using an internal standard (Y) and two different Al emission lines. The ¹⁰Be/⁹Be ratios were measured at Lawrence Livermore National Laboratory and normalized to primary standard 07KNSTD3110, assuming a ¹⁰Be/⁹Be ratio of 2.85 x 10⁻¹² (ref. 33). ²⁶Al/²⁷Al ratios were measured at Purdue Rare Isotope

Measurement Laboratory and normalized to KNSTD standard 26Al-1-05-2 with an assumed 26 Al/ 27 Al ratio of 1.82 x 10^{-12} (ref. 34). Isotopic data are given in Supplementary Data.

Blanks. Two procedural blanks were prepared with the samples during nuclide extraction to estimate background nuclide abundances resulting from both laboratory sample processing and AMS analysis. To characterize more fully the possible range of backgrounds, we also considered all blanks run by the same operator in the same fume hood (dedicated exclusively to the preparation of low-ratio samples) with other long-buried samples from beneath the Greenland Ice Sheet (n=26 for ¹⁰Be, n=18 for ²⁶Al) (Supplementary Data). We quantify the central tendency and dispersion of the sample and blank populations using their arithmetic means and standard errors. All blanks were measured at the same AMS facilities as the samples (Lawrence Livermore National Laboratory for ¹⁰Be, Purdue Rare Isotope Measurement Laboratory for ²⁶Al).

Statistical analysis. Traditionally, Frequentist methods (i.e., null-hypothesis significance tests) are applied (e.g., t-test) to the sample results and process blanks to determine whether the two groups are statistically different or if individual samples are statistically distinct from a group of blanks. A null hypothesis is framed (e.g., "the true mean of the samples is less than or equal to the true mean of the blanks") and is rejected for p values less than the significance level (α). However, under a Frequentist approach, one cannot express *support* for the research hypothesis (e.g., that a given sample result is greater than the mean of the blanks). A low p-value simply means there is a low chance that our data would support the null hypothesis simply by random chance⁵⁸. In other words, the probability of incorrectly rejecting the null (Type I error) is low. On the other hand, a Bayesian analysis can support either a null or research hypothesis, provide explicit information about the precision of parameter estimations in the form of credible

intervals, and allow data to be examined in the context of the effect size³⁵⁻³⁷. Bayesian frameworks have the added advantage of allowing for non-normal distribution of data sets³⁸, which can be a common occurrence when working with low-level detection samples³⁹. Notably, our AND-1B data sets exhibit some non-normality. While ¹⁰Be blanks and samples and ²⁶Al blanks were each from a normal distribution as confirmed by Shapiro-Wilks test (at a significance level, α , of 0.05), the group of ²⁶Al blanks was not normally distributed.

Bayesian inference was applied to estimate distribution parameters (including the mean and standard deviation) for our AND-1B data sets, and compare parameters between the samples and blanks. In the context of the t-test, our response variables (10 Be and 26 Al reported in the samples and the blanks) were modeled as having a t-distribution to accommodate potential outliers. The t-distribution is similar to a normal distribution, parameterized by mean (μ) and standard deviation (σ), but includes a third parameter (ν) that accommodates heavy-tailed distributions (ν <30) and near-normal distributions (ν =30).

Model parameters included μ_1 , μ_2 σ_1 , σ_2 , ν , with the subscripts denoting the identity of the blanks (Group 1) and samples (Group 2). Non-informative priors were assigned to each parameter. A normal distribution was assigned to μ_1 , μ_2 centered on the empirical mean of pooled data (both blank and sample groups), with a variance ranging from 0.2 to 5 times the standard deviation of the pooled data. Standard deviation parameters, σ_1 , σ_2 , were each assigned a prior distributed as a gamma density with shape and rate parameters "derived from the desired *mode* and standard deviation of the gamma distribution"⁵¹. Equal normality was assumed for both groups, with a prior for ν distributed as a gamma density with shape and rate parameters "derived from the desired *mean* and standard deviation of the gamma distribution"⁴⁰.

Gibbs sampling was used to obtain samples from the posterior distribution and estimate the mean, standard deviation, standard error of the mean (SEM), mode, quantiles and credible intervals for each Bayesian model parameter. Markov-chain Monte Carlo sampling was implemented in R⁴¹ using the "BEST" package⁴², which relies on "JAGS"⁴³ and "coda"⁴⁴. Sampling was conducted with three chains, for 100,000 iterations with a thinning factor of 1, after discarding the initial 4,500 iterations for adaptation and burn-in phases. Convergence was confirmed by visual examination of trace plots and the Gelman-Ruben statistic⁴⁵ (i.e., potential shrink reduction factor less than 1.1).

We first compared the blanks to samples for each nuclide (expressed in atoms), applying a one-sided, two-group t-test (2GTT) using both Frequentist and Bayesian approaches. Importantly, our blank results included all laboratory process blanks run alongside low-level samples in the same hood by the same operator over time (n=26 for ¹⁰Be and n=18 for ²⁶Al).

A Frequentist one-sided, 2GTT (unequal variances, Welch approximation) determined that the mean of the samples may be greater than the mean of the blanks for both 10 Be and 26 Al. The null hypothesis (that the true mean of the samples is less than or equal to the true mean of the blanks) was rejected at $\alpha = 0.05$ (p < 0.05, Extended Data Table 1).

A Bayesian, one-sided, 2GTT yielded consistent results, but provided support for the research hypothesis (i.e., that the sample mean is greater than the blank mean) and quantified the probability. Results indicate the two groups (samples vs. blanks) are credibly different for both ¹⁰Be and ²⁶Al; and there is a greater than 99% probability that the sample mean is greater than the blank mean for each nuclide (Extended Data Table 1). The 95% credible interval on the estimated *difference* between group means excludes zero for both ¹⁰Be and ²⁶Al.

Next, we compared each individual sample to the mean of the blanks to determine if the samples contained credible quantities of ¹⁰Be and ²⁶Al, using both Frequentist and Bayesian methods. The two methods yielded contrasting outcomes with the value of Bayesian over Frequentist methods becoming especially apparent from this analysis.

The Frequentist 1GTT was performed to evaluate the null hypothesis that the sample result was less than or equal to the blank mean. For ¹⁰Be, a low p value (<0.10) was obtained for seven of the eight samples (A through G), rejecting the null hypothesis. However, this 1GTT failed to reject the null hypothesis for reported ¹⁰Be in sample H. For ²⁶Al, a low p value (<0.10) resulted in a rejection of the null hypothesis for all eight samples. However, Frequentist analysis does not permit us to express support for the research hypothesis – i.e., that ²⁶Al is credibly present in these eight samples, or that ¹⁰Be is credibly present in seven of the eight samples - only that there is a low probability of a Type I error.

Bayesian 1GTT were carried out by defining a Region of Uncertainty (ROU) around the sample-specific estimate equal to \pm 10. Bayesian 1GTT results indicated that \pm 10 Be is credibly present above the mean blank value in seven of the eight samples (all but H). In each credible case, the blank mean is less than the sample value, and a 90% Credibility Interval (C.I.) on the posterior distribution of the mean of the blanks fully excludes the \pm 10 ROU surrounding the sample value (Extended Data Fig. 8a). In contrast, for sample H, the mean of the blanks is greater than the reported sample value (Extended Data Fig. 8b). An estimated 92.9% of the posterior distribution is above the sample value, and 89.9% of the posterior distribution of the mean is located within the sample-specific ROU (Extended Data Table 2).

In the case of ²⁶Al, Bayesian 1GTT results indicated this constituent is credibly present above the mean blank value in samples B, C, E, F, G and H only. In contrast, samples A and D

may be, to varying degrees, indistinguishable from the process blanks (Extended Data Table 2). While the 90% C.I. on the posterior distribution of the blank mean was less than, and fully excluded, the respective sample value, a percentage of the posterior distribution (17.5% and 10.8%, respectively, for A and D) was located within the sample-specific ROU – including portions of the 90% C.I. (Extended Data Fig. 8c).

Thus, Bayesian 1GTT results contrast with those of the Frequentist null-hypothesis significance tests. While significant p values (at $\alpha = 0.10$) obtained in the Frequentist 1GTT may have led one to conclude that 10 Be is present in seven out of eight samples and 26 Al is present in all eight samples with a "confidence" interval of 90%, we can only state a low chance of having incorrectly rejected a true null hypothesis (i.e., generated a "false positive") for these samples. The Bayesian approach, however, allowed us to express *support* for the research hypothesis that 10 Be is credibly present above the mean of the blanks in samples A-G, and 26 Al is credibly present above background only in samples B, C, E, F, G, and H.

It is difficult to explain the presence of ²⁶Al but the absence of ¹⁰Be in sample H given the shorter half-life of ²⁶Al. Because ²⁶Al abundance in this sample barely exceeds the threshold for statistical significance (Fig. 3b), we consider it dubious that this sample in fact contains measurable ²⁶Al and disregard it.

Blank correction. To estimate the concentration of nuclides in the samples, we subtracted the mean nuclide abundance of all the blanks. We quantified the blank uncertainty as the standard error of the mean, and combined it with the measurement uncertainty of the sample nuclide abundances in quadrature.

Decay correction. We corrected measured cosmogenic nuclide concentrations for radio-decay on the seafloor following deposition using the age model from Wilson et al.²⁷, which is based on

paleomagnetic events, biostratigraphic data, and 40 Ar/ 39 Ar ages. Because measurements were made on amalgamated subsamples spanning considerable depth (and thus age) ranges in the core, we used the average age of the subsamples, weighted by their sand (>125 μ m) masses. Our cosmogenic record is relatively insensitive to age model uncertainties because the age uncertainties are substantially smaller than the half-lives of 10 Be and 26 Al (1.39 (ref. 46) and 0.71 Myr (ref. 47)).

Limiting initial nuclide concentrations of blank-level samples. We estimated the maximum concentration that samples without measurable nuclides could have had when they were deposited and still decayed to blank levels by today. For example, our average 10 Be blank has \sim 7,000 atoms. This implies that the oldest sample (H), which does not have measurable 10 Be, could have had up to \sim 380,000 atoms (or \sim 19,000 atoms/g for this 20.1 g sample) when it was deposited 8 Ma (5.75 half lives ago).

Antarctic erosion rates. The AND-1B cosmogenic nuclide record is erosion-weighted because sediments are sourced from areas in proportion to their erosion rate. In addition, areas of more rapid erosion contribute deeper-sourced, and thus nuclide-poorer, material, potentially diluting the cosmogenic nuclide concentration resulting from a past exposure event. Modeling, sediment backstacking techniques, subglacial imaging, and thermochronometry suggest that while Antarctic subglacial erosion rates may have reached up to 200 m/Myr in spatially isolated regions in the past, spatial averages were typically much lower (1-2 m/Myr)⁴⁸⁻⁵⁰, particularly during the late Cenozoic as landscape dissection probably slowed with colder conditions and less aggressive glacial erosion^{49,51,52}.

Modeling hypothetical exposure scenarios. We generated synthetic ¹⁰Be and ²⁶Al records to help inform interpretation of the AND-1B record using the MATLAB implementation of

Heisinger et al.⁵³ and Balco et al.⁵⁴, including nuclide production by muons. In a first experiment, we evaluated whether the ²⁶Al measured in our record could have been produced prior to EAIS expansion at 14 Ma, and find that it could not. For instance, even in an extreme scenario with a high-elevation, non-eroding surface saturated with ²⁶Al (equal rates of nuclide production and loss by radio-decay) at 14 Ma and subsequently decaying for 20 half-lives under cold-based, non-erosive ice cover, there would not be detectable ²⁶Al remaining today (Extended Data Fig. 4). In a second set of simulations, we calculated ¹⁰Be and ²⁶Al concentrations in sediment eroded from a bedrock profile averaged over multiple glacial cycles, driven by high-latitude production rates at sea level and 2000 m asl, and given various durations of exposure per cycle (0-100%) and glacial erosion rates (0-100 m Myr⁻¹). AND-1B Pliocene ¹⁰Be concentrations are consistent with exposure lasting >10% of a glacial cycle only in cases with low-elevation sediment sources and very high erosion rates; most scenarios in agreement with the AND-1B data instead imply little to no exposure during the Pliocene, and especially the Pleistocene (Extended Data Fig. 5). Lastly, we tested whether a single episode of exposure for 10, 50, 100, or 200 kyr during the mid-Pliocene could yield a ¹⁰Be record similar to ours. We assumed that the bedrock had no cosmogenic nuclides initially, rock was eroded at various rates (0, 20, and 100 m Myr⁻¹) and the resulting sediment transported instantaneously to the sea floor, where the radionuclides were only subject to decay. The resulting time series were degraded to the resolution of our isotopic record. The simulations suggest that both short-exposure, low-erosion and long-exposure, higherosion scenarios could yield ¹⁰Be concentrations similar to the AND-1B Pliocene samples, but the rapid erosion in the latter scenarios decreases ¹⁰Be concentrations more quickly than we observe during the Pleistocene (Extended Data Fig. 6). The long mid-Pliocene exposure scenario would require either a substantial decrease in erosion rates from the Pliocene to the Pleistocene

or continued brief exposure events during the Pleistocene to match the entire AND-1B record. We also repeated the 200 kyr mid-Pliocene exposure simulation, but first mixed eroded bedrock into a deformable till layer before fluxing it to the ocean. We used deformable bed thicknesses of 1 and 10 m, erosion rates of 10 and 80 m Myr⁻¹, assumed instantaneous homogenization of eroded bedrock material throughout the deformable bed in each time step, and removed an equal amount of bed material to the ocean to keep the bed thickness constant. This sediment mixing reduces the magnitude of the mid-Pliocene exposure signal and extends its longevity through time compared to the bedrock-only simulations, but it similarly fails to replicate the AND-1B record; high erosion rates are needed to reduce Pliocene ¹⁰Be concentrations in the regolith to AND-1B values, but low erosion rates are needed to slowly discharge the regolith to the ocean over the past several million years (Extended Data Fig. 6). More complicated scenarios would be required to fit the AND-1B record, such as long-lived pockets of higher-¹⁰Be regolith mixing with more rapidly eroding, and thus lower-¹⁰Be, bedrock.

Data availability. All AND-1B data generated in this study (sediment processing, sample and blank isotopic ratios and concentrations) are provided as Supplementary Data.

Code availability. The codes used to model cosmogenic nuclide exposure and erosion scenarios shown in the Extended Data Figures are available at https://github.com/shakunj/Shakun-et-al-2018-Nature.

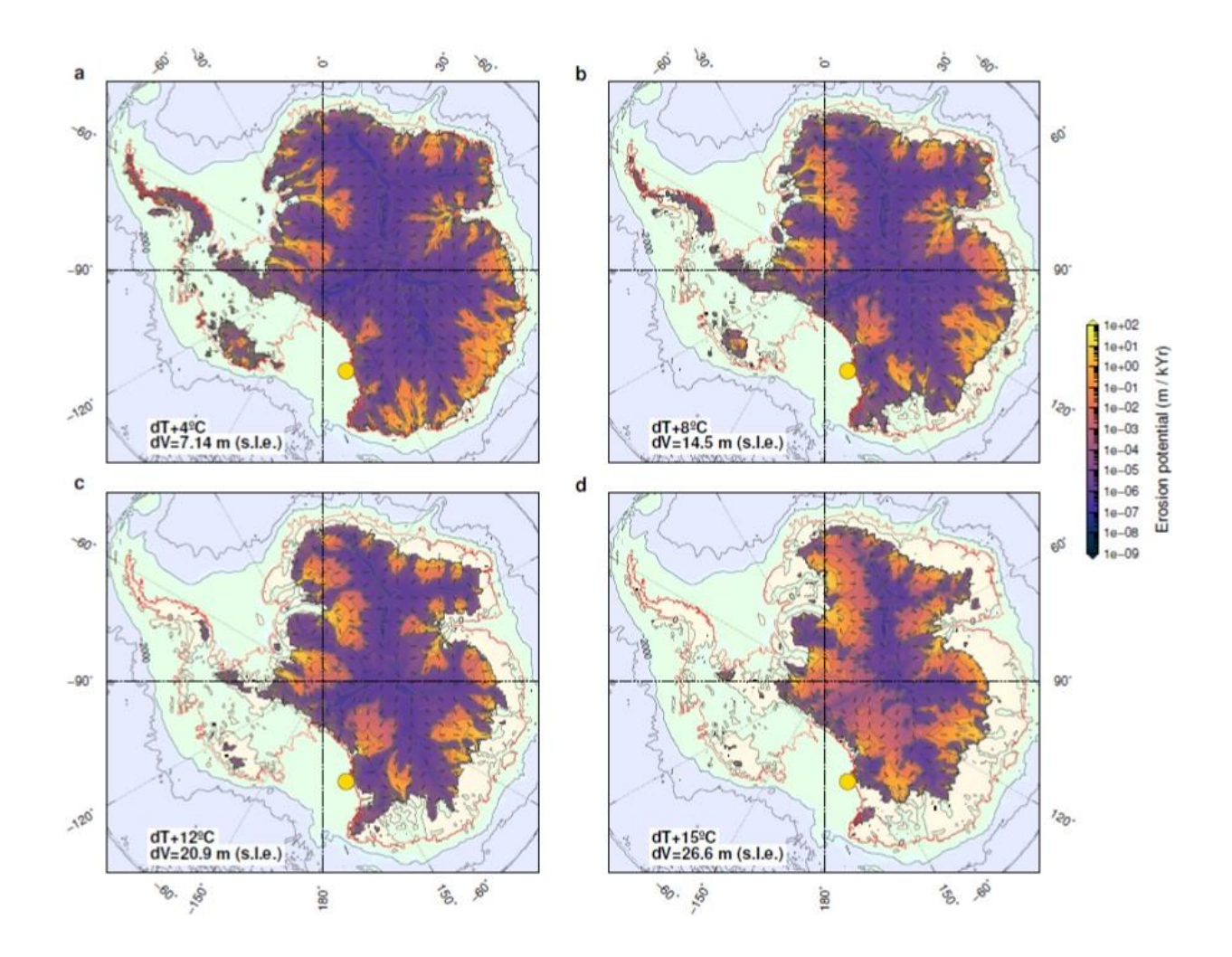
- 31 Krissek, L. *et al.* Sedimentology and stratigraphy of the AND-1B core, ANDRILL McMurdo Ice Shelf Project, Antarctica. *Terra Antarctica* **14**, 185-222 (2007).
- Corbett, L. B., Bierman, P. R. & Rood, D. H. An approach for optimizing in situ cosmogenic 10Be sample preparation. *Quaternary Geochronology* **33**, 24-34 (2016).

- Nishiizumi, K. *et al.* Absolute calibration of 10Be AMS standards. *Nuclear Inst. and Methods in Physics Research, B* **258**, 403-413 (2007).
- Nishiizumi, K. Preparation of 26Al AMS standards. *Nuclear Instruments and Methods in Physics Research Section B: Beam Interactions with Materials and Atoms* **223–224**, 388-392 (2004).
- 35 Nuzzo, R. Statistical errors. *Nature* **506**, 150-152 (2014).
- Kruschke, J. K. Bayesian estimation supersedes the t test. *Journal of Experimental Psychology* **142**, 573-603 (2013).
- 37 Kruschke, J. K. *Doing Bayesian data analysis: a tutorial with R, JAGS and Stan.* (Elsevier, 2015).
- 38 Gelman, A., Carlin, J. B., Stern, H. S. & Rubin, D. B. Bayesian Data Analysis.
 (Chapman & Hall/CRC, 2004).
- Currie, L. A. The Measurement of Environmental Levels of Rare Gas Nuclides and the Treatment of Very Low-Level Counting Data. *IEEE Transactions on Nuclear Science* **19**, 119-126, doi:10.1109/TNS.1972.4326496 (1972).
- 40 Kruschke, J. K. in *Doing Bayesian Data Analysis* Vol. 2017 (2015).
- 41 Team, R. C. D. *R: A language and environment for statistical computer*, http://www.R-project.org/ (2016).
- 42 Kruschke, J. K. & Meredith, M. *BEST: Bayesian Estimation Supersedes the t-Test*, https://cran.r-project.org/web/packages/BEST/index.html (2015).
- Plummer, M. in *Proceedings of the 3rd international workshop on distributed statistical computing (dsc 2003).*

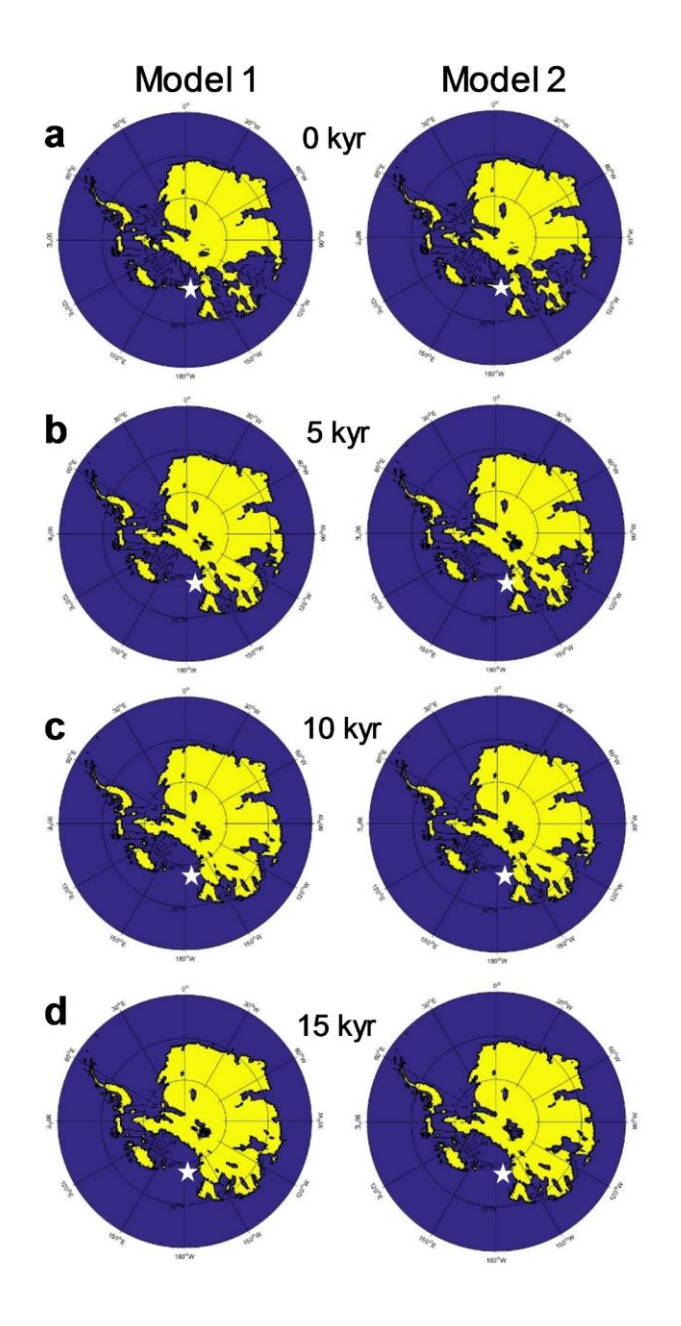
- Plummer, M., Best, N., Cowles, K. & Vines, K. CODA: convergence diagnosis and output analysis for MCMC. *R News* **6**, 7-11 (2006).
- Gelman, A. & Rubin, D. B. Inference from Iterative Simulation Using Multiple Sequences. *Statist. Sci.* **7**, 457-472, doi:10.1214/ss/1177011136 (1992).
- Korschinek, G. et al. A new value for the half-life of 10Be by Heavy-Ion Elastic Recoil Detection and liquid scintillation counting. *Nuclear Instruments and Methods in Physics Research Section B: Beam Interactions with Materials and Atoms* **268**, 187-191 (2010).
- Norris, T. L., Gancarz, A. J., Rokop, D. J. & Thomas, K. W. Half-life of 26Al. *Journal of Geophysical Research: Solid Earth* 88, B331-B333, doi:10.1029/JB088iS01p0B331 (1983).
- Jamieson, S. S. R., Sugden, D. E. & Hulton, N. R. J. The evolution of the subglacial landscape of Antarctica. *Earth and Planetary Science Letters* **293**, 1-27, doi:10.1016/j.epsl.2010.02.012 (2010).
- Thomson, S. N., Reiners, P. W., Hemming, S. R. & Gehrels, G. E. The contribution of glacial erosion to shaping the hidden landscape of East Antarctica. *Nature Geosci* 6, 203-207, doi:10.1038/ngeo1722 (2013).
- Wellman, P. & Tingey, R. J. Glaciation, erosion and uplift over part of East Antarctica.

 Nature 291, 142-144 (1981).
- Bo, S. *et al.* The Gamburtsev mountains and the origin and early evolution of the Antarctic Ice Sheet. *Nature* **459**, 690-693, doi:10.1038/nature08024 (2009).
- Young, D. A. *et al.* A dynamic early East Antarctic Ice Sheet suggested by ice-covered fjord landscapes. *Nature* **474**, 72-75, doi:10.1038/nature10114 (2011).

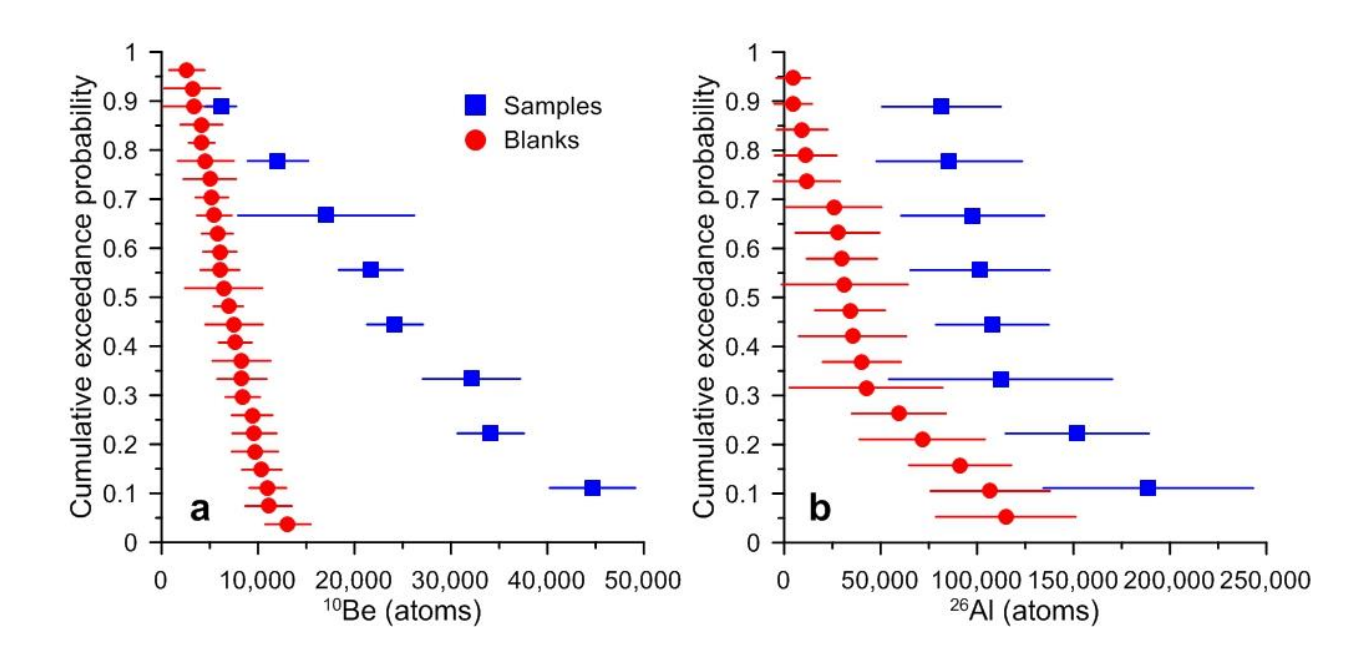
- Heisinger, B. *et al.* Production of selected cosmogenic radionuclides by muons. *Geochimica et Cosmochimica Acta* **66**, A558 (2002).
- Balco, G., Stone, J. O., Lifton, N. A. & Dunai, T. J. A complete and easily accessible means of calculating surface exposure ages or erosion rates from 10Be and 26Al measurements. *Quaternary Geochronology* **3**, 174-195, doi:10.1016/j.quageo.2007.12.001 (2008).



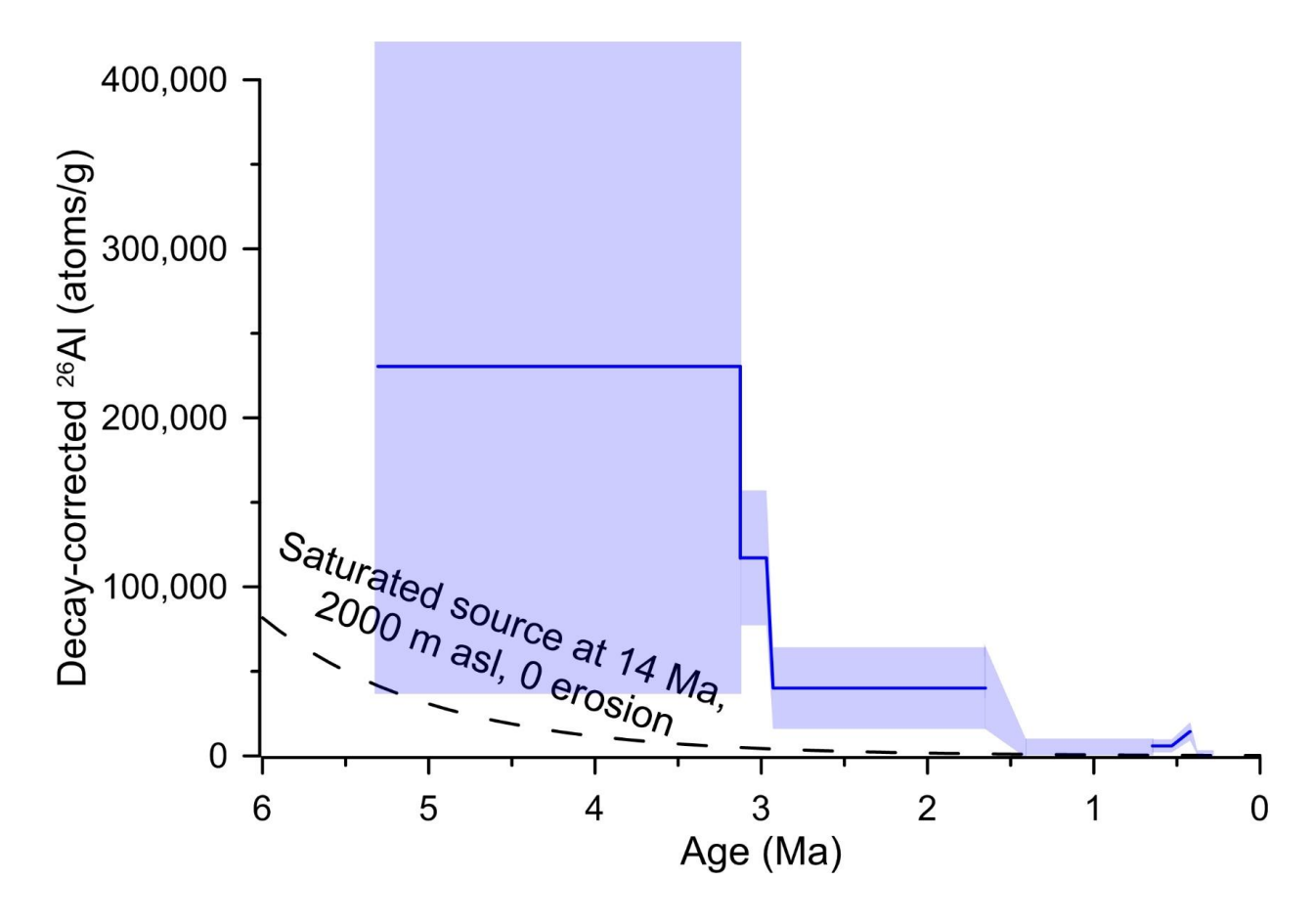
Extended Data Figure 1. Modeled patterns of erosion. Simulated erosion potential under the Antarctic Ice Sheet calculated from modeled driving stress and basal velocity fields for several uniform (atmosphere and ocean) warming scenarios of (a) 4°C, (b) 8°C, (c) 12°C, and (d) 15°C ⁵⁵. The location of the AND-1B core is shown by the yellow dot. Note that erosive zones tend to extend toward the continental interior with warming.



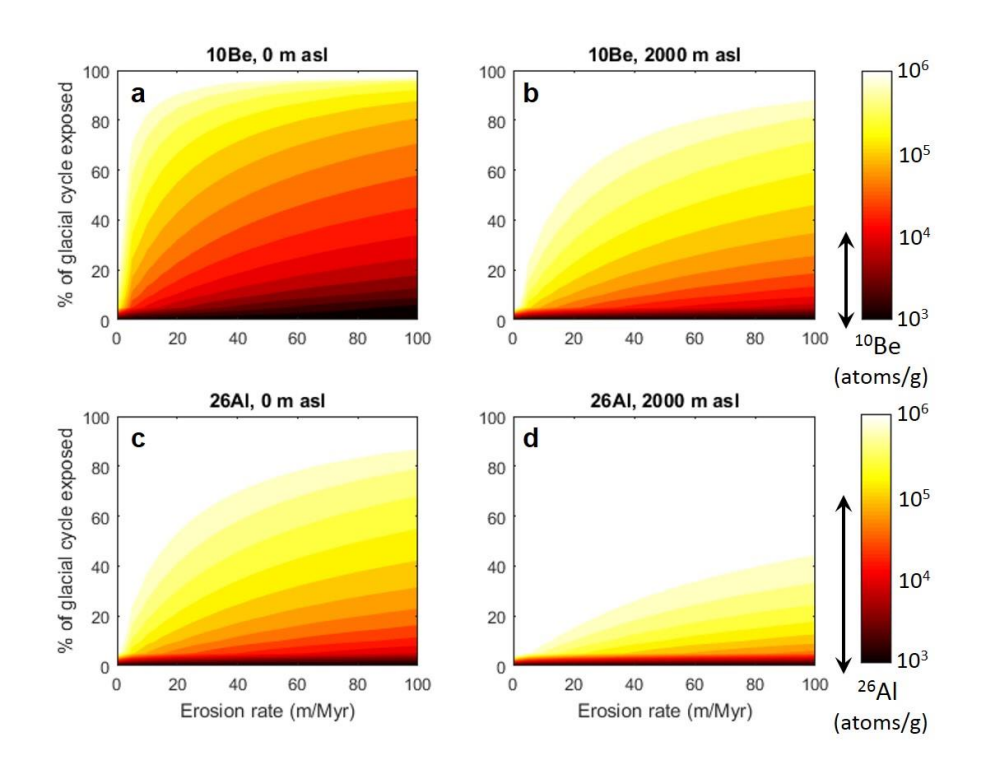
Extended Data Figure 2. Glacial isostatic adjustment following ice retreat. Antarctic land above sea level (yellow) (a) 0, (b) 5, (c) 10, and (d) 15 kyr after a near-instantaneous (1-kyr) collapse of all marine-based ice sheet sectors for two different mantle viscosity models²⁶. Model 1 is from Peltier et al.⁵⁶, and Model 2 has the following parameters: lithosphere thickness = 96 km, upper mantle viscosity = 5×10^{20} Pa s, lower mantle viscosity = 10^{22} Pa s. The location of the AND-1B core is shown by the star.



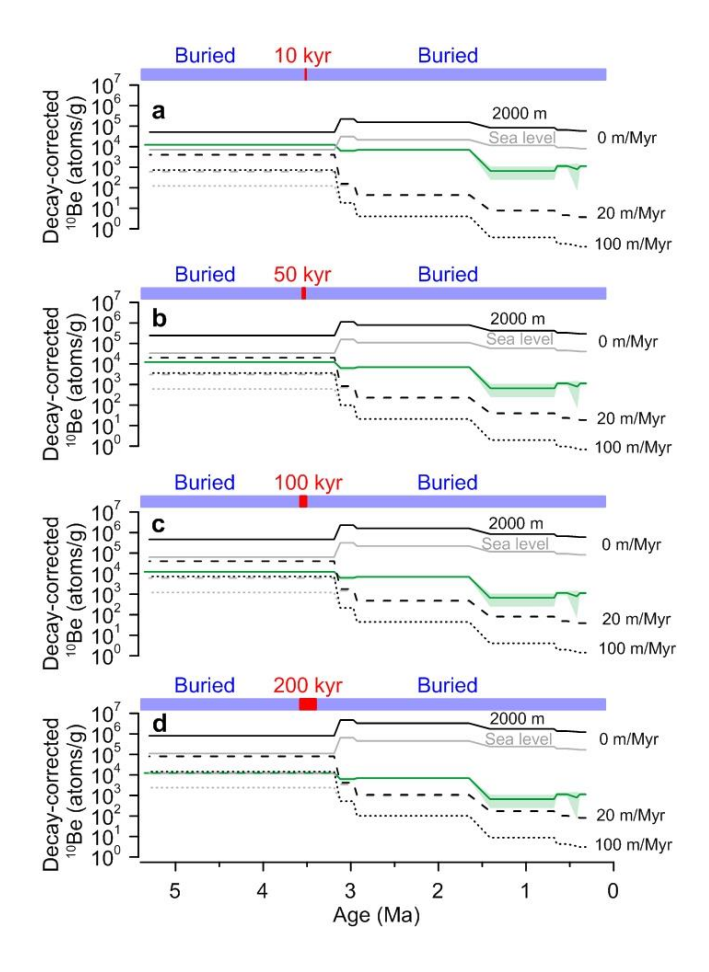
Extended Data Figure 3. AND-1B sample versus blank populations. Cumulative exceedance probabilities of measured (i.e., not blank-corrected) (a) ¹⁰Be and (b) ²⁶Al nuclide abundances in AND-1B samples (blue) and all blanks run by the same operator in the same low-level hood (red), with 1σ uncertainties. These plots display the fraction of measurements that exceed a given nuclide abundance. Note that probabilities are generally higher for the samples than the blanks; in other words, a random draw from the samples is more likely to be above a random draw from the blanks, suggesting that they are separable populations.



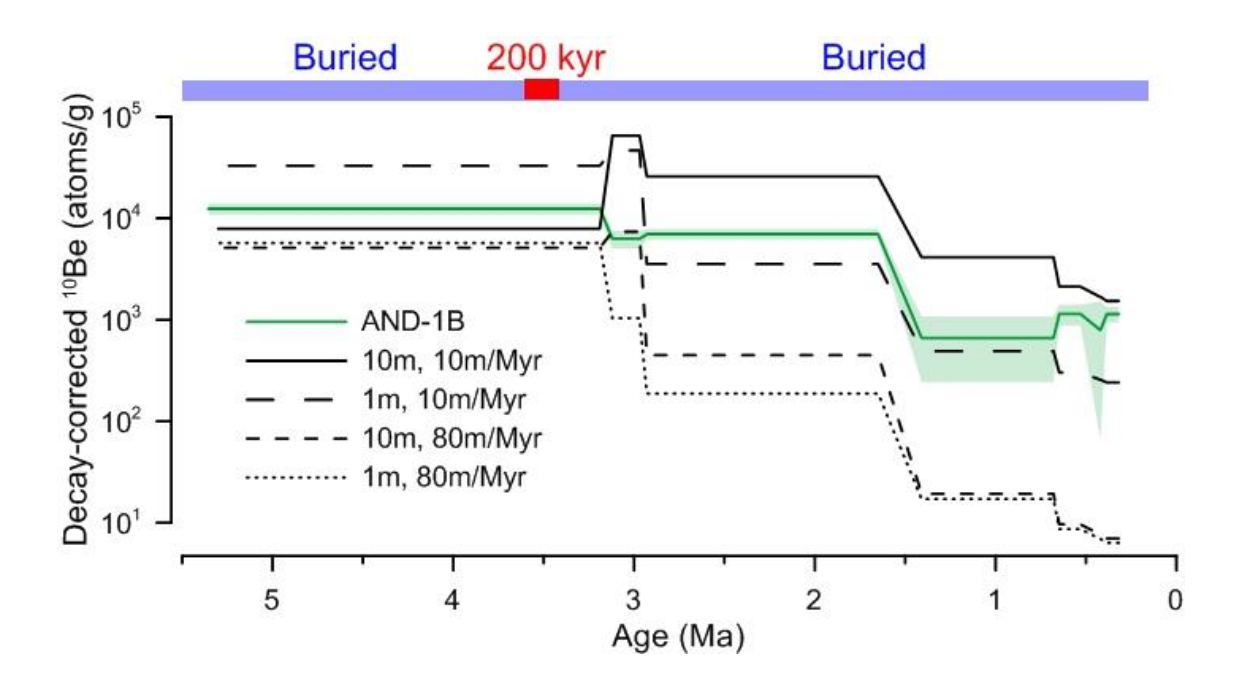
Extended Data Figure 4. AND-1B decay-corrected ²⁶Al concentrations. Shaded intervals surrounding the blue line show 1σ uncertainties, while shaded intervals not surrounding the blue line show the possible range of decay-corrected concentrations in samples that are below detection limit. The dashed black line simulates the ²⁶Al concentration in non-eroding material at 2000 m asl that was originally saturated at 14 Ma and subsequently decayed under cold-based, non-erosive ice. The fact that several AND-1B samples have higher concentrations than even this extreme scenario most favorable to having nuclides persist to the present suggests that the AND-1B nuclides were produced after the expansion of the EAIS in the mid-Miocene.



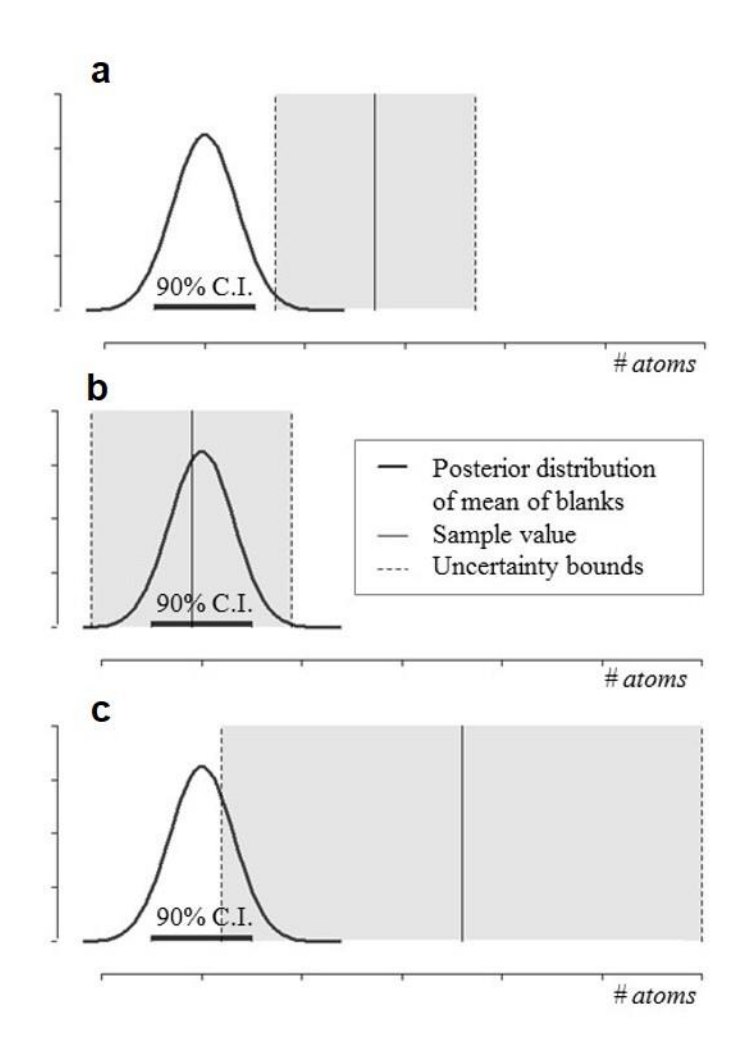
Extended Data Figure 5. Modeled cosmogenic nuclide concentrations for various interglacial exposure durations and glacial erosion rates. Simulated (**a,b**) ¹⁰Be and (**c,d**) ²⁶Al concentrations in material sourced from sea level and 2000 m asl in Antarctica as a function of the fraction of time land is exposed over 40 kyr glacial cycles. Results are nearly identical for 100 kyr cycles. Erosion rates were assumed to be 0 m/Myr during ice-free conditions, based on geologic evidence for negligible late Cenozoic erosion in ice-free areas of the TAM^{9,10}. Black arrows next to the scale bars show the range of decay-corrected nuclide concentrations in AND-1B samples. The model was initialized with zero nuclides at 8 Ma (representative of conditions implied by AND-1B sample H), assumes instantaneous transport of eroded sediment to the ocean and no mixing, and continuous radio-decay. Concentrations shown are the Pliocene (5-3 Ma) average. Comparison of these simulations with AND-1B nuclide concentrations suggests that land exposure in sediment source regions was probably quite limited in duration and/or extent through the Plio-Pleistocene.



Extended Data Figure 6. Modeling a mid-Pliocene exposure event of bedrock. Each panel shows AND-1B decay-corrected ¹⁰Be concentrations with 1σ uncertainty (green), as well as simulated ¹⁰Be concentrations assuming a single (a) 10 kyr, (b) 50 kyr, (c) 100 kyr, and (d) 200 kyr exposure of a bedrock column in the mid-Pliocene. The exposure event was chosen to start at 3.6 Ma and extend up to 200 kyr in duration based on the presence of a 60-m thick diatomite unit in the AND-1B core thought to reflect warm interglacial conditions from 3.6-3.4 Ma¹. Simulated records are driven by production at sea level (gray) or 2000 m asl (black), and subjected to continuous radio-decay and continuous erosion at rates of 0 m/Myr (solid lines), 20 m/Myr (dashed lines), and 100 m/Myr (dotted lines). The model assumes that the sediment source was initially devoid of nuclides and that sediments are transported instantaneously to the sea floor. The synthetic time series have been binned to the same resolution as the AND-1B data.



Extended Data Figure 7. Modeling a mid-Pliocene exposure event with eroded bedrock mixed through a deformable bed. AND-1B decay-corrected ¹⁰Be concentrations with 1σ uncertainty (green), as well as simulated ¹⁰Be concentrations assuming a single exposure event from 3.6-3.4 Ma and routing of eroded bedrock through a well-mixed deformable bed for various bed thicknesses and erosion rates. Material eroded from the bedrock profile is instantaneously mixed throughout the deformable bed in each time step, and an equal amount of material is removed from the bed, keeping its thickness constant. Sediment mixing in the deformable bed dilutes the surface ¹⁰Be signal of the exposure event but extends its longevity through time in comparison to the bedrock simulations shown in Extended Data Fig. 6. Simulated records are driven by production at sea level, and subjected to continuous radio-decay and continuous erosion. The model assumes that the bedrock and deformable bed were initially devoid of nuclides and that sediments eroded from the deformable bed are transported instantaneously to the sea floor. The synthetic time series have been binned to the same resolution as the AND-1B data.



Extended Data Figure 8. Conceptual diagram of Bayesian one-group t-test outcomes and their interpretation. (a) Nuclide is credibly present above background: i.e., the sample value is greater than the mean of the blanks (defined at the mode of the posterior distribution), and the region of uncertainty surrounding the sample value fully excludes the 90% credible interval (C.I.) on the posterior distribution of the mean of the blanks; (b) Nuclide is not credibly present above background: the sample value is less than or equal to the blank mean; (c) Nuclide is not credibly present above background: while the sample value is greater than the blank mean, the region of uncertainty surrounding the sample value does not fully exclude the 90% C.I.

Test		¹⁰ Be		²⁶ Al		
	Blanks (10 ³ atoms)	Samples (10 ³ atoms)	Two-sample, one- sided t-test (α=0.05)	Blanks (10 ⁴ atoms)	Samples (10 ⁴ atoms)	Two-sample, one- sided t-test (α=0.05)
Frequentist [†]	7.05±0.54 n=26	24.01±4.45 n=8	Frequentist: p = 0.0033*	4.18±0.80 n=18	11.59±1.29 n=8	Frequentist: p < 0.0001*
			Rejects H ₀ (that mean of the samples is less than or equal to the mean of the blanks)			Rejects H ₀ (that mean of the samples is less than or equal to the mean of the blanks)
Bayesian [‡]	7.02±0.58 n=26	23.91±5.92 n=8	Bayesian: 99.4% probability that sample mean is greater than the blank mean	3.98±0.89 n=18	11.40±1.68 n=8	Bayesian: 99.9% probability that sample mean is greater than the blank mean

Extended Data Table 1. Comparison of nuclide abundances in sample populations with procedural blank populations. ¹Arithmetic mean and standard error of the mean of samples and of all blanks associated with hood in which samples were processed by same operator. ²Bayesian estimation of mean and standard error of the mean of samples and of all blanks associated with hood in which samples were processed by same operator. ³The mean and standard error values estimated under Frequentist and Bayesian methods differ slightly, given that the former is derived arithmetically and the latter is derived through MCMC sampling.

¹⁰ Be								
Sample	Measured (10 ³ atoms)	Corrected with blanks using Freq mean/SEM $\left(10^3 \text{ atoms}\right)^\dagger$	Frequentist one- sample t-test $(\alpha=0.10)^{\ddagger}$	Corrected with blanks using Bayes mean/SEM (10 ³ atoms) [¶]	Bayesian one-sample t- test 90% Credible Interval / ROU = $1\sigma^{1}$			
A	24.21±2.91	17.16±2.96	p < 0.10*	17.19±2.97	0/0/Y			
В	17.06±9.13	10.01±9.15	p < 0.10*	10.04±9.15	0/5.7/Y			
C	21.68±3.33	14.63±3.38	p < 0.10*	14.66±3.38	0/0/Y			
D	12.07±3.14	5.02±3.18	p < 0.10*	5.05±3.19	0/0.1/Y			
E	44.67±4.45	37.62±4.49	p < 0.10*	37.65±4.49	0/0/Y			
F	32.12±5.05	25.07±5.08	p < 0.10*	25.10±5.08	0/0/Y			
G	34.11±3.46	27.06±3.51	p < 0.10*	27.09±3.51	0/0/Y			
H	6.167±1.58	- 0.88±1.67	p = 0.943	- 0.85±1.68	92.9/89.9/N			

²⁶ Al								
Sample	Measured (10 ⁴ atoms)	Corrected with blanks using Freq mean/SEM $\left(10^4 \text{ atoms}\right)^\dagger$	Frequentist one- sample t-test (α=0.10) [‡]	Corrected with blanks using Bayes mean/SEM (10 ⁴ atoms) [¶]	Bayesian one-sample test 90% Credible Interval / ROU = 1σ ¹			
A	8.56±3.77	4.39±3.86	p < 0.10*	4.59±3.88	0/17.5/N			
В	18.87±5.44	14.69±5.50	p < 0.10*	14.89±5.51	0/0/Y			
C	9.77±3.71	5.59±3.79	p < 0.10*	5.80±3.81	0/1.3/Y			
D	8.15±3.08	3.97±3.18	p < 0.10*	4.17±3.21	0/10.8/N			
E	10.15±3.61	5.97±3.70	p < 0.10*	6.18±3.72	0/0.4/Y			
F	15.19±3.72	11.02±3.80	p < 0.10*	11.22±3.82	0/0.0/Y			
G	11.21±5.79	7.03±5.85	p < 0.10*	7.23±5.86	0/5.4/Y			
H	10.79±2.92	6.61±3.02	p < 0.10*	6.81±3.05	0/0.0/Y			

Extended Data Table 2. Comparison of nuclide abundances in individual samples with procedural blanks. ¹Arithmetic average of blanks subtracted from measured atoms in each sample, with uncertainties added in quadrature. In calculating the blank average, a value of one-half the lowest detected blank value was substituted for two of the eighteen ²⁶Al blanks which exhibited zero-count results. ²Test result is significant at specified alpha level, where indicated by *. Test compared non-corrected samples individually to the mean of the blanks. ³Bayesian-estimated blank mean subtracted from measured atoms in each sample, with uncertainties added in quadrature, using Bayesian estimated standard error of the mean (SEM) of the blanks. ⁴Values formatted as "a/b/c" represent the following statistics: a – percent of the posterior distribution of the mean of the blanks above the sample value, b – percent of the posterior distribution of the mean of the blanks within the region of uncertainty (ROU) around the sample value. ROU defined as +/- 1 σ , c – Y = yes, N = no in answer to the question "constituent credibly present in sample?" (i.e., 90% Credibility Interval of posterior distribution of the mean of the blanks is less than and fully excludes the ROU around the sample value?).

- Golledge, N. R., Levy, R. H., McKay, R. M. & Naish, T. R. East Antarctic ice sheet most vulnerable to Weddell Sea warming. *Geophysical Research Letters* **44**, 2343-2351, doi:10.1002/2016GL072422 (2017).
- Peltier, W. R. Global glacial isostasy and the surface of the Ice-Age Earth: The ICE-5G (VM2) model and GRACE. *Annual Review of Earth and Planetary Sciences* **32**, 111-149 (2004).